J Mater Sci (2007) 42:5999–6003
DOI 10.1007/s10853-006-1119-z

Finite element analysis of microimprinting of bulk metallic glasses in supercooled liquid regime

M. Cheng · S. H. Zhang · J. A. Wert

Received: 30 August 2005 / Accepted: 10 October 2006 / Published online: 6 April 2007

Abstract A finite element analysis (FEA) model to analyze imprint of a bulk metallic glass (BMG) in the temperature range near the glass transition temperature (T_g) has been developed. The material model includes both Newtonian and non-Newtonian flow behavior. The results reveal that the topology of the imprinted surface depends strongly on temperatures, but only mildly on surface feature scale. As a result of the flow characteristics of BMG in the temperature range above T_g, the lubrication condition has only a slight effect on BMG imprinting.

Introduction

Bulk metallic glasses exhibit large viscous flow in the supercooled liquid regime (SLR) [1–5]. The flow enables fabrication of precision 3D structures at the micro scale. Although the bulk metallic glasses have been extensively studied, a few studies have been carried out on modeling of forming processes of BMG [6, 7]. Previously published models focus on particular geometries without broadly exploring variations of friction coefficient, surface feature size, and BMG properties. This paper presents FEM model results for a simple imprinting geometry in conjunction with a material model, which was proposed to describe non-Newtonian as well as Newtonian behavior of several BMG, including $Mg_{60}Cu_{30}Y_{10}$.

M. Cheng (✉) · S. H. Zhang
Institute of Metal Research, Chinese Academy of Sciences, Shenyang 110016, China
e-mail: mcheng@imr.ac.cn

J. A. Wert
Materials Research Department, Risø National Laboratory, Roskilde 4000, Denmark

Material model

Kawamura and coworkers [8] reported that the temperature (T) and strain rate ($\dot{\varepsilon}$) dependence of viscosity (η) for BMG in the Newtonian flow regime at temperatures significantly above T_g, and the non-Newtonian flow regime at temperatures near T_g, can be expressed by a stretched exponential function of the form

$$\eta = B\exp\left(\frac{H}{RT}\right)\left[1-\exp\left(\frac{D}{\{\dot{\varepsilon}C\exp(H^*/RT)\}^{\beta}}\right)\right]. \quad (1)$$

The factors B, H, D, C, H^* and β are material constants, and R is the gas constant. For a uniaxial applied stress (σ), the constitutive relation for viscous flow is written

$$\eta = \frac{\sigma}{3\dot{\varepsilon}}. \quad (2)$$

The data reported by Wert et al. [9] for an $Mg_{60}Cu_{30}Y_{10}$ BMG have been analyzed to determine the material constants appearing in Table 1. Values reported earlier for $Zr_{65}Al_{10}Ni_{10}Cu_{15}$ and $Pd_{40}Ni_{40}P_{20}$ [8] are also shown in the table. Note that the values listed for D in Table 2, Ref. [8] give negative viscosity when substituted into Eq. 5, Ref [8]. This error is corrected in Table 1 of the present article where the values listed are $-1/D$ from Table 2, Ref. [8]. The values in the last column of Table 1 are the extrapolated viscosities at the crystallization temperature, T_x.

Table 1 Material parameters for viscosity relation

Alloy composition	Refs.	B (Pa s)	H (KJ/mol)	C (s)	H^* (KJ/mol)	D	β	$\eta(T_x)$ (Pa s) [10]
$Mg_{60}Cu_{30}Y_{10}$	[9]	5.0×10^{-24}	274	7.0×10^{-29}	230	–0.050	0.40	7.0×10^{5}
$Zr_{65}Al_{10}Ni_{10}Cu_{15}$	[8]	8.4×10^{-19}	363	3.1×10^{-21}	261	–0.0049	0.84	3.0×10^{8}
$Pd_{40}Ni_{40}P_{20}$	[8]	2.4×10^{-42}	580	7.0×10^{-26}	278	–0.012	0.82	7.0×10^{5}

By algebraic manipulation and approximation of the exponential function by the first two terms of a series expansion, Eqs. 1, 2 can be expressed

$$\dot{\varepsilon} \cong \left[\frac{1}{3B}\exp(-H/RT)\right]\sigma + \left[\left\{\frac{-C^{\beta}}{3BD}\exp\left(\frac{\beta H^{*}-H}{RT}\right)\right\}^{\frac{1}{1-\beta}}\right]\sigma^{\frac{1}{1-\beta}}. \tag{3}$$

The first term of Eq. 3 describes the Newtonian flow behavior observed at low strain rates and temperatures significantly above T_g. The second term describes non-Newtonian flow observed at higher stresses and lower temperatures. At fixed temperature, Eq. 3 has the general form

$$\dot{\varepsilon} = A_1\sigma^{n_1} + A_2\sigma^{n_2}, \tag{4}$$

where A_1, n_1, A_2, n_2 are obtained from to the more complex expressions in Eq. 3. Figure 1 shows the characteristic flow curves of $Mg_{60}Cu_{30}Y_{10}$ amorphous alloy in the supercooled liquid state and the data reported by Wert et al. [9].

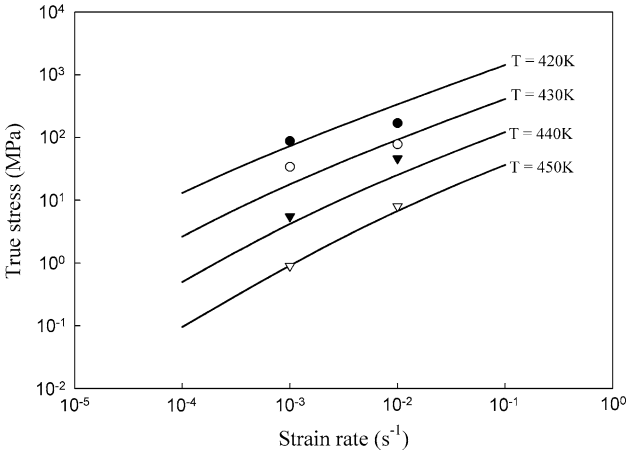

Fig. 1 Characteristic flow curves of $Mg_{60}Cu_{30}Y_{10}$ amorphous alloy in the supercooled liquid state and the data reported by Ref. [9]

FEA model

Model geometry

Figure 2 illustrates the die and material geometry used in this study. An imprinting die with a series of V-grooves of opening width W, depth W, and center-to-edge spacing S is envisaged. Figure 2 shows a portion of a die with $W/S = 0.2$. From symmetry considerations, the plane-strain model analyzes can be confined to the range $0 < x < 0.5S$. The height of the workpiece was taken as $0.4S$. Load was applied via a punch at the top of workpiece. The model geometry was implemented using the ABAQUS® standard program package; Fig. 2 shows the initial 2D FE mesh. The simple form of Eq. 4 is compatible with the ABAQUS® user subroutine CREEP. The punch and die were considered to be rigid and no material flow was allowed across the boundaries at $x = 0$ and $x = 0.5S$. The groove corner was rounded to avoid singularities in the model results; the parameter R/S is the radius of curvature of the corner normalized by S. The friction coefficient between the workpiece and the die, and the workpiece and the punch (μ), was specified in the range $0 \le \mu \le 0.5$.

In the model, imprinting is effected by a fixed velocity applied by the rigid punch at a reference point (arrow at

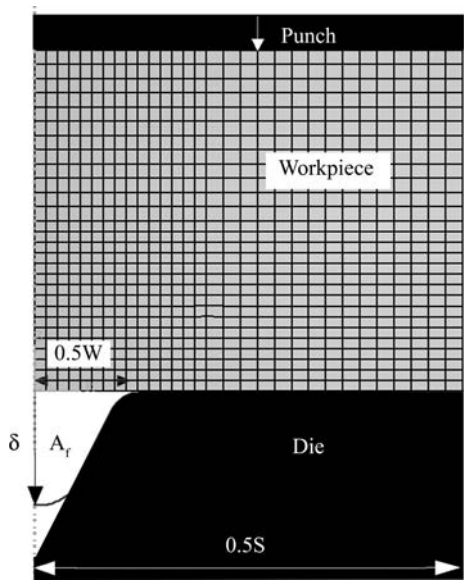

Fig. 2 Die, workpiece, and punch configuration used in the present model. The initial FE mesh is superposed on the workpiece. The curved lines in the groove show model results at certain imprinting time for fully amorphous $Mg_{60}Cu_{30}Y_{10}$ imprinted. The parameter δ describes the extent of material flow at the groove centerline

the top of Fig. 2). Since the punch is constrained to remain horizontal, the point selected for application of the load is immaterial. This loading scheme has the advantage that the load per unit length along the punch was able to vary with position in accordance with the requirements of equilibrium, closely simulating experimental conditions. Constant applied pressure model results were also obtained. Various element types were employed in a trial phase of the project. Slight differences in the predicted geometry of the imprinted surface were found when different element types were chosen. All results shown in the present article were obtained using elements of type CPE4R. Imprinting was considered to be isothermal; the material model was described in Section ''Material model''. Surface tension effects, which could be significant for imprinting of very fine scale features, are not incorporated into the present model.

Model results

Detailed model results consist of maps showing material flow and stress as functions of position and time during the imprinting process. From a practical perspective, however, the significant process result is the surface topology. The parameter δ/W (Fig. 2) represents the normalized maximum distance of material flow into a die groove. A second parameter, A_f/A_g, (Fig. 2) represents the filled area fraction of the V-groove whose total area is represented by A_g. In the present work, δ/W and A_f/A_g are used as parameters representing the imprinted surface topology.

Figure 3a is a plot of δ/W as a function of maximum imprinting pressure for $Mg_{60}Cu_{30}Y_{10}$ at four temperatures, for constant punch velocity simulations. Figure 3b is a plot of A_f/A_g as a function of maximum imprinting pressure for $Mg_{60}Cu_{30}Y_{10}$ at four temperatures, for constant punch velocity simulations. The initial FE meshes and corner radius of curvature were constant for these analyzes shown in Fig. 3. For the simple groove geometry used in the present study, the plots of δ/W and A_f/A_g are quite similar. In the following, the parameter A_f/A_g is used because the normalized imprinted area is more easily generalized to different groove geometries.

Figure 4a is a plot of A_f/A_g as a function of maximum imprinting pressure for $W/S = 0.2$ but variable radius of curvature at the groove corner. These results demonstrate that the corner radius does not have a significant effect on the imprinting process with BMG. Figure 4b is a plot of A_f/A_g as a function of maximum imprinting pressure for $R/S = 0.04$ but a range of W values. Figure 4b shows that the values of A_f/A_g for imprinting with various groove widths ($0.1 \leq W/S \leq 0.4$) lie along a single curve. This suggests that imprinting with BMG is not very sensitive with the width of the imprinted features.

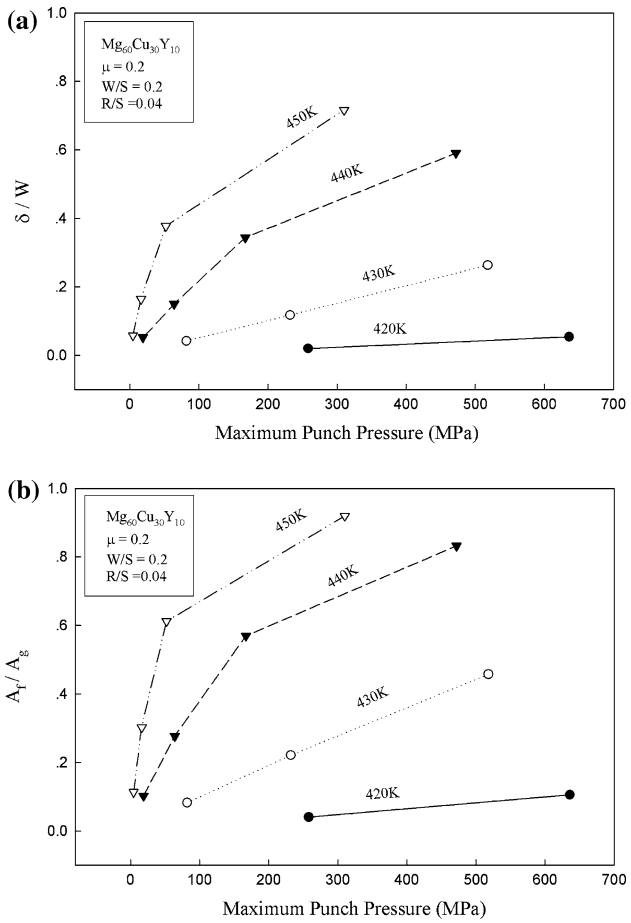

Fig. 3 (**a**) δ/W as a function of maximum punch pressure and temperature. (**b**) A_f/A_g as a function of maximum punch pressure and temperature. W/S and R/S are fixed for both sets of calculations

Figure 5 shows A_f/A_g vs. pressure, friction coefficient (μ) and temperature (T) for constant imprinting pressure simulations with $Mg_{60}Cu_{30}Y_{10}$, and illustrates the strong effect of temperature on BMG imprinting. The friction coefficient is seen to have a weak effect on BMG imprinting.

Figure 6 shows A_f/A_g vs. pressure and BMG composition, for constant imprinting pressure simulations and illustrates the strong effect of BMG composition on the imprinting process. The imprinting temperature was selected in each case as a temperature at which forming experiments have successfully been conducted in previous investigations [10–12].

Discussion

Figure 3b shows that the imprinting process for BMG is highly temperature sensitive. The temperature sensitivity is greatest in the range near T_g where the material exhibits

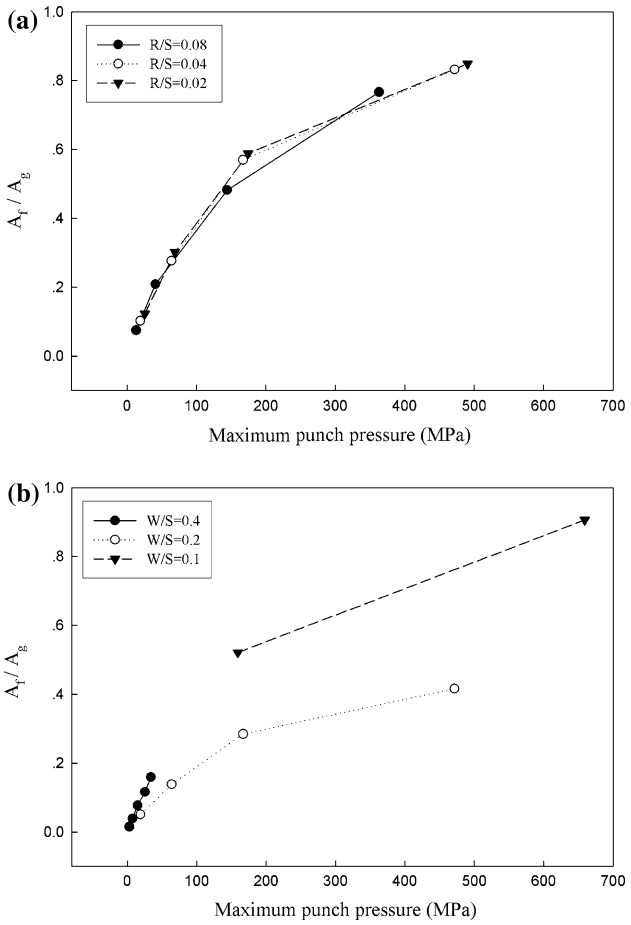

Fig. 4 (**a**) A_f/A_g as a function of maximum punch pressure and the geometrical parameter *R/S*. (**b**) A_f/A_g as a function of maximum punch pressure and the geometrical parameter *W/S*. Temperature (440 K) and friction coefficient (0.2) are fixed for both sets of calculations

Non-Newtonian flow to a greater degree. Once the alloy has been heated into the temperature range where mainly Newtonian flow is observed, the temperature sensitivity of the imprinting process is reduced.

The mild influence of the friction coefficient on BMG imprinting, Fig. 5, is a prominent result of the imprinting model. This result disagrees with the suggestion in a prior publication that friction affected the pressure required for microextrusion of a $La_{55}Al_{25}Ni_{20}$ BMG [13]. The SEM micrographs of microextrudates in the earlier article revealed that the length of extruded material was smaller than or roughly equal to its width. Thus, the microextrusion process reported by Saotome and Iwazaki [13] was geometrically quite similar to the microimprinting process being considered here. There is no evidence in Ref. [13] that the friction condition was varied, so the earlier suggestion is most likely an extension to BMG of traditional metalworking experience, which suggests that friction strongly influences extrusion.

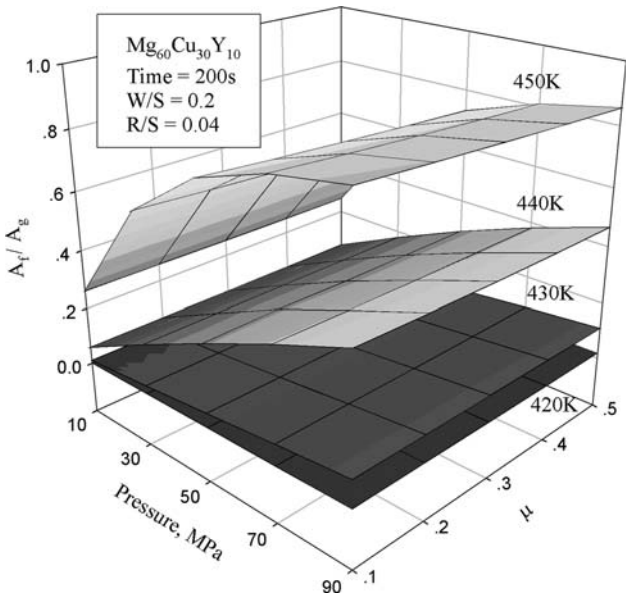

Fig. 5 A_f/A_g as a function of imprinting pressure and friction coefficient

The strong effect of BMG composition on the forming process is also a prominent result. This finding supports an earlier suggestion that the viscosity at the crystallization temperature, $\eta(T_x)$, is a useful index of BMG formability [9]. Values of $\eta(T_x)$ for the three BMG evaluated in the current modeling study are listed in the last column of Table 1. Comparison of these values with Fig. 6 shows that $\eta(T_x)$, is approximately correlated with imprintability. While the values of $\eta(T_x)$ suggest similar imprintability for $Mg_{60}Cu_{30}Y_{10}$ and $Pd_{40}Ni_{40}P_{20}$, Fig. 6 indicates that $Pd_{40}Ni_{40}P_{20}$ exhibits superior imprintability. The difference can be attributed to the smaller temperature interval between T_g and T_x for $Mg_{60}Cu_{30}Y_{10}$ than for $Pd_{40}Ni_{40}P_{20}$, which requires $Mg_{60}Cu_{30}Y_{10}$ to be imprinted at a

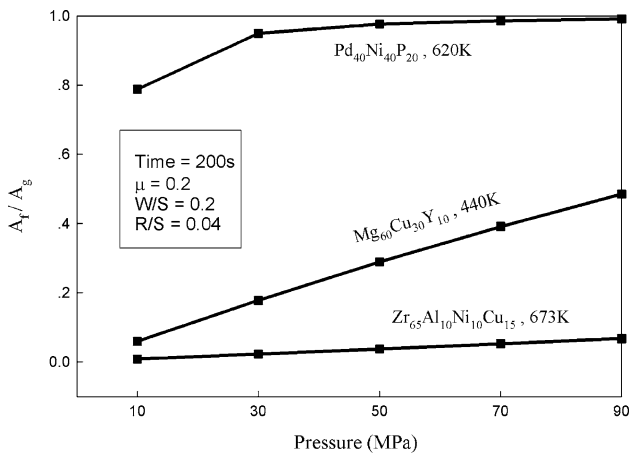

Fig. 6 A_f/A_g as a function of imprinting pressure for three BMG

temperature rather close to T_g. Thus, $\eta(T_x)$ can only be considered as an approximate guide for imprintability. It is also worth noting that, although $Pd_{40}Ni_{40}P_{20}$ exhibits better imprintability than $Mg_{60}Cu_{30}Y_{10}$ at the temperatures used for model evaluation, the higher T_g of $Pd_{40}Ni_{40}P_{20}$ (578 K [8]) imposes more severe high temperature die strength requirements than for $Mg_{60}Cu_{30}Y_{10}$ (437 K [9]).

Conclusions

FEA modeling of the imprinting process for BMG reveals the following conclusions.

1. The surface topology depends strongly on temperature but only mildly on surface feature scale during the BMG imprinting process.
2. As a result of the flow characteristics of BMG in the temperature range above T_g, the lubrication condition has a mild influence on BMG imprinting.
3. The viscosity at the crystallization temperature is confirmed by model results as a useful indicator of BMG imprintability.

Acknowledgements The authors express sincere appreciation to the DANIDA Fellowship Program for financial support during the course of this work. We are grateful to N. Pryds for experimental assistance; to A. Schrøder Pedersen, M. Eldrup, Erik Johnson for thoughtful comments.

References

1. Nieh TG, Wadsworth J, Liu CT, Ohkubo T, Hirotsu Y (2001) Acta Mater 49:2887
2. Saotome Y, Itoh K, Zhang T, Inoue A (2001) Scripta Mater 44:1541
3. Kawamura Y, Nakamura T, Inoue A, Masumoto T (1999) Mater Trans JIM 40:794
4. Kawamura Y, Itoi T, Nakamura T, Inoue A (2001) Mater Sci Eng A 304–306:735
5. Saotome Y, Imai K, Shioda S, Shimizu S, Zhang T, Inoue A (2002) Intermetallics 10:241
6. Kim HS, Kato H, Inoue A, Chen HS (2004) Acta Mater 52:3813
7. Kim HS, Kato H, Inoue A, Chen HS, Hong SI (2004) Mater Trans 45:1228
8. Kawamura Y, Nakamura T, Kato H, Mano H, Inoue A (2001) Mater Sci Eng A 304–306:674
9. Wert JA, Pryds NH, Zhang E (2001) In: Dinesen AR, Eldrup M, Juul Jensen D, Linderoth S, Pederson TB, Schrøder Pederson A, Wert JA (eds) Proceedings of the 22nd Risø International Symposium on Materials Science, Risø (DK), September 2001, p 423
10. Chu JP, Chiang CL, Nieh TG, Kawamura Y (2002) Intermetallics 10:1191
11. Reger-Leonhard A, Heilmaier M, Eckert J (2000) Scripta Mater 43:459
12. Pryds NH (2004) Mater Sci Eng A 375–377:186
13. Saotome Y, Iwazaki H (2001) J Mater Process Technol 119:307